Giant negative domain wall resistance in iron

Dieter Elefant and Rudolf Schäfer*
Leibniz Institute for Solid State and Materials Research Dresden (IFW Dresden), Helmholtzstrasse 20, D-01069 Dresden, Germany
(Received 26 September 2010; published 25 October 2010)

By manipulating the magnetic domains of high-purity bulk iron single crystals (characterized by residual resistance ratios up to 5700) in small magnetic fields, resistivity changes up to a factor of 100 are measured at low temperature. Domain observation by Kerr microscopy shows that domain wall creation and annihilation is the origin of the resistivity changes. A qualitative model is suggested in which the walls act as channels for the electric current due to specific Lorentz trajectories around the walls. It is expected that this *fundamental* negative wall resistance effect contributes to magnetoresistance phenomena in any material and device containing domain walls.

DOI: 10.1103/PhysRevB.82.134438 PACS number(s): 72.15.Gd, 75.47.−m, 75.60.Ch

I. INTRODUCTION

The discovery of the giant magnetoresistance (GMR) (Refs. 1 and 2) has stimulated intensive search for an intrinsic electrical resistance effect that is caused by the walls between ferromagnetic (fm) domains because of the analogy of the magnetization configuration around domain walls to that in GMR multilayers. The central question in these studies addresses the influence of the magnetization rotation within a domain wall [Fig. 1(a)] on the spin of the conduction electrons, eventually creating a domain wall resistance (DWR) due to spin-dependent scattering. By manipulating the domain structure in a defined manner, mostly in magnetic films, one tries to extract such an intrinsic DWR from all the other, superimposed resistivity terms in the fm material that can be summarized as

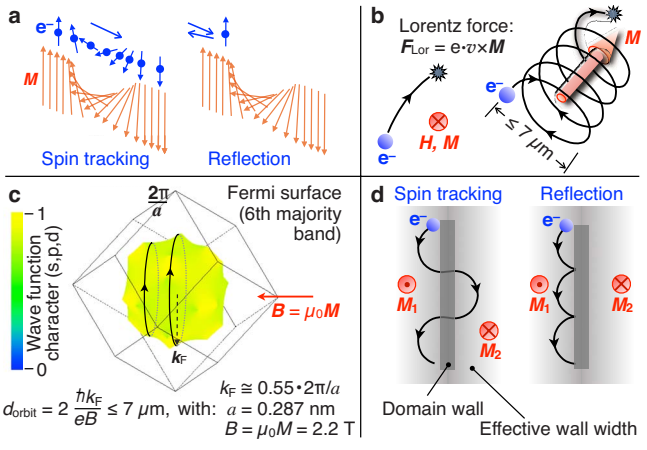

FIG. 1. (Color online) Fundamental diagrams: (a) scheme of the interaction of an electron [with magnetic moment (spin) ↑ and charge e^-] and a classical Bloch-type domain wall. When the electron passes a wide wall its spin can change direction according to the wall magnetization (translation with spin tracking), whereas reflection with spin conservation will preferably occur for narrow walls. The latter effect is expected to cause a positive domain wall resistance. (b) Electron trajectories in real space due to the Lorentz force, shown for small (left) and large mean-free paths (right). (c) Fermi-surface sheet of iron (Ref. 3) with sketches of two cyclotron orbits caused by the magnetization $\boldsymbol{M}$ for large relaxation times. (d) Lorentz trajectories along a domain wall, schematically shown for the cases of spin tracking and reflection.

$$\rho = \rho_0 + \rho(T) + \rho_{\mathrm{DWR}} + \rho_{\mathrm{AMR}} + \Delta\rho_{\mathrm{Lorentz}}. \quad (1)$$

Here ρ_0 is the residual resistance due to scattering on lattice defects and impurities, and $\rho(T)$ is a temperature-dependent term due to quasiparticle scattering on phonons etc. The anisotropic magnetoresistance ρ_{AMR} (Ref. 4) depends on the angle between magnetization $\boldsymbol{M}$ and electrical current and is typically about 1% of $\rho_0+\rho(T)$. Via the Lorentz force, $\boldsymbol{M}$ bends the electron trajectories [Fig. 1(b)] thus causing the Lorentz MR (LMR) $\Delta\rho_{\mathrm{Lorentz}}$.[5–7] Additive size effects in films are ignored in Eq. (1).

The measured DWR in magnetic films typically yields magnitudes in the promille range of the total resistance and differs even in the sign of the effect (compare, e.g., Refs. 8 and 9—here a "positive" DWR means an increase in resistance due to the presence of a domain wall, and vice versa for "negative" DWR). DWR effects are obviously tiny effects and it seems difficult to separate them from the other, usually larger resistivity contributions. The current state of knowledge can be summarized by citing the conclusions of two reviews on this subject: "at present a consensus of the observability of the DWR has not been reached"[10] and "… there is an extensive literature going back many decades where the resistance of domain walls has been measured. It seems fair to say that most of these experiments have not detected intrinsic effects, but voltages caused by other changes in the electric field with domain structure due to anisotropic MR, Kohler MR, or Hall effects have been measured."[11]

In this paper a MR effect is presented that (relatively) exceeds the effects in Eq. (1) by orders of magnitude. Phenomenologically it is a *negative DWR* (NDWR), caused by the formation of channels for the charge carriers around domain walls that can "shortcut" the domain resistance $\Delta\rho_{\mathrm{Lorentz}}$. If the walls have an orientation component along the net direction of the electrical current, the shortcut effect thus leads to a reduction in the LMR. This fundamental influence of domain walls on the electric transport was not considered in the literature on magnetoresisivity so far. The discovery was possible by choosing samples which allow the clear separation of all superimposed, "parasitic" resistivity and MR effects by (temperature-dependent) resistance measurements and controlled domain manipulation. The samples

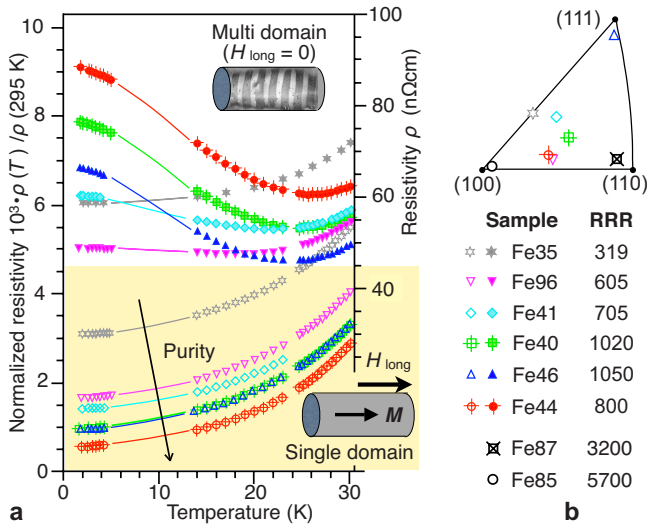

FIG. 2. (Color online) (a) Temperature dependence of resistivity for six iron crystals, plotted in reduced [left ordinate, $\rho(295\ \mathrm{K})=9.71\ \mu\Omega\ \mathrm{cm}$] and absolute units (right ordinate). The lower set of curves was measured in the longitudinally saturated state ($\mu_0 H_{\mathrm{long}} \cong 100$ mT), the upper set in some multidomain states at $\mu_0 H_{\mathrm{circ}} \cong 0.8$ mT. (b) Sample legend, together with residual resistance ratios RRR (see text) and stereographic plot showing the crystallographic orientations of the rod axes.

were bulk single-crystalline iron rods with different crystallographic orientations and of extremely high physical and chemical perfection that has, to our best knowledge, hitherto not been reported. They are specified in Sec. II together with the methods for resistivity measurement and domain observation. The combined interpretation of temperature- and field-dependent resistivity data (Sec. III) together with the domain studies (Sec. IV) reveals the significant role of domain walls for the drastic resistivity changes measured. In Sec. V the NDWR is phenomenology described based on arguments that are derived from fermiology. Section VI summarizes the paper. In order to "streamline" the main text, we have added elaborate material in the appendices of the paper that addresses specific points that are more of interest for specialists in electric transport and magnetic domains, but that are important to fill gaps in the chain of arguments of the main text.

II. MATERIALS AND METHODS

Eight cylindrical iron single-crystal rods with different crystallographic orientations and a polycrystalline rod were investigated. The rods had diameters of 1–4 mm and lengths between 17 and 60 mm. An overview of the monocrystalline samples is given in Fig. 2(b). The crystals were of high purity and lattice perfection, characterized by residual resistance ratios $\mathrm{RRR}=\rho(295\ \mathrm{K})/\rho(T\approx 2\ \mathrm{K})$ up to 5700, which are the highest values for bulk iron reported so far. The extraordinary quality of our crystals was achieved by a sequence of several preparation and characterization steps including chemical and physical purification. Finally single crystals were grown by the strain-anneal technique.[12–15] Due to the crystal perfection, the coercivity $\mu_0 H_{\mathrm{coercive}}$ of our crystals is smaller than 0.1 mT.

The electrical resistance was measured by a four-probe direct-current (dc) method. Alternating current methods could not be applied because of possible magnetic viscosity effects and the necessity to generate static circular "self-fields" H_{circ} by the measuring current J along the rods. In our experiments these circular fields were also used as a tool to reorient the magnetic domains. At the rod surface they are estimated to $\mu_0 H_{\mathrm{circ}}=\mu_0 J/\pi D$ (D is the rod diameter). The dc-measuring currents ranged between some milliampere and 10 A with maximum current densities of $10^7\ \mathrm{Am}^{-2}$. The electrical contacts were made by spot welding of Ni wires (potential probes) and Ni plates (current contacts) to the crystals, realizing contact resistances smaller than 10 $\mu\Omega$. Due to the bulk dimensions of the crystals and their high purity, the absolute sample resistances scale down to the 100 nΩ range. To extract the true sample potential, the direct current had to be converted several times for every measuring point to eliminate thermoelectric (often time-dependent) voltages in the measuring circuit. The dc-voltage detection limit was better than 1 nV.

A serious point is the sample temperature. Currents up to 10 A can introduce significant Joule's heat into the crystals up to the 10^{-3} W range via the contact resistances. To avoid heating, most low-temperature measurements were performed by immersing the samples into liquid helium ($T=1.9$–4.9 K), parahydrogen ($T=14.0$–23.0 K), and neon ($T=23.6$–30.0 K). By vapor pressure regulation, stable temperatures with $\Delta T\approx 0.01$ K could be realized for all ranges. Small longitudinal magnetic fields up to $\mu_0 H=0.12$ T were applied along the rod axis (parallel J) by coils within the cryogenic liquids or by a Weiss magnet. Additive measurements, using a variable temperature insert in a superconducting 16 T magnet, were restricted to currents $J\leq 100$ mA to avoid Joule's heat.

The measured low-temperature resistance values $R(T)$ were normalized to the room-temperature resistance of each sample,

$$r(T)=R(T)/R(295\ \mathrm{K})\cong\rho(T)/\rho(295\ \mathrm{K}). \qquad (2)$$

Thus with $\rho(295\ \mathrm{K})=9.71\times 10^{-8}\ \Omega$ m for pure bulk iron[16] the low-temperature specific resistivity $\rho(T)$ could be determined without geometrical sample uncertainties.

The domain structure and its change in magnetic fields was observed by Kerr microscopy. So the resistivity measurements $\Delta\rho(B)$ could be interpreted in terms of the magnetization changes $B=\mu_0(H+M)$. For domain imaging, the longitudinal Kerr effect, which is sensitive to in-plane magnetized surface domains, was applied in a wide field polarization microscope enhanced by image processing.[17] Only a limited portion of the curved rod surface could be imaged in focus but by suspending the rods on a rotational stage the whole surface was accessible. *In situ* magnetic fields and electrical currents could be applied during microscopy. The domain observations have been performed at room temperature, whereas the resistivity measurements are low-temperature experiments. The domain studies can nevertheless be applied for the interpretation of the electrical data.

Though the material parameters that determine the domain character (anisotropy constant, saturation magnetization, and magnetostriction constant) have different magnitudes at low temperature, they do not change in sign compared to room temperature. Therefore the domain *character* is expected to be largely temperature independent in the investigated regime. Also the effect of sample heating by applying measuring currents does not have a significant influence on the domains. The highest current applied in imaging experiments was 5 A for a few minutes at most. The sample temperature rises by some 10°, depending on the time the current is applied. This rise has no influence on the domain character—the domains and magnetization processes remain the same, independently whether we freshly start the experiment or whether we perform domain studies after having heated the crystals by applying currents for a while.

III. TEMPERATURE AND FIELD DEPENDENCE OF RESISTIVITY

Figure 2(a) shows for selected crystals the temperature dependence of resistivity in multidomain and in longitudinally saturated single domain states. Remarkable features are noted: (i) in the single domain state the $\rho(T)$ dependence is similar to that of nonmagnetic materials. (ii) The absolute resistivities increase up to a factor of 20 from the saturated to the multidomain states. (iii) The large resistivities in the multidomain states drop with increasing temperature, an effect that has not been reported so far for pure bulk ferromagnetic material. (iv) The higher the chemical and crystallographic perfection, the larger the effects (the influence of the crystallographic orientation is superimposed though).

In Fig. 3 the resistivity dependence on small applied circular and longitudinal fields is plotted for the (100) and (110) crystals. Reference state for the H_{circ} experiments is the longitudinally saturated state, the resistance $\rho_{\mathrm{sat}}^{\mathrm{long}}(T)$ of which is indicated by lines in Fig. 3(a). Removing the saturation field, the resistivity rises by factors as can be seen by comparing the $\rho_{\mathrm{sat}}^{\mathrm{long}}(T)$ lines with the $H_{\mathrm{circ}}=0$ values in Fig. 3(a). For increasing circular field, Figs. 3(a) and 3(b) reveal a further resistivity increase by factors—the application of small circular fields of just 2 mT obviously causes a drastic resistivity change up to a factor of 100 for the (100) and a factor of 30 for the (110) crystal compared to the longitudinal single domain reference state [the different factors are primarily due to the different RRR of the crystals, see Fig. 2(b)]. Superimposing then a longitudinal field of the same order of magnitude, nearly all the giant resistivity increase is canceled [Fig. 3(c)]. An interpretation of these effects requires knowledge of the domain structures.

IV. DOMAIN STUDIES

Figure 4 shows the domains on the (110) crystal for some states along the curves in Fig. 3. According to Fig. 4(a) there are six easy crystal directions for $\boldsymbol{M}$: the [100], [$\bar{1}$00] directions, which we call ±90° directions as they are at 90° relative to the current axis, and the [010], [0$\bar{1}$0], [001], and [00$\bar{1}$] directions called ±45° and ±135° directions. In a

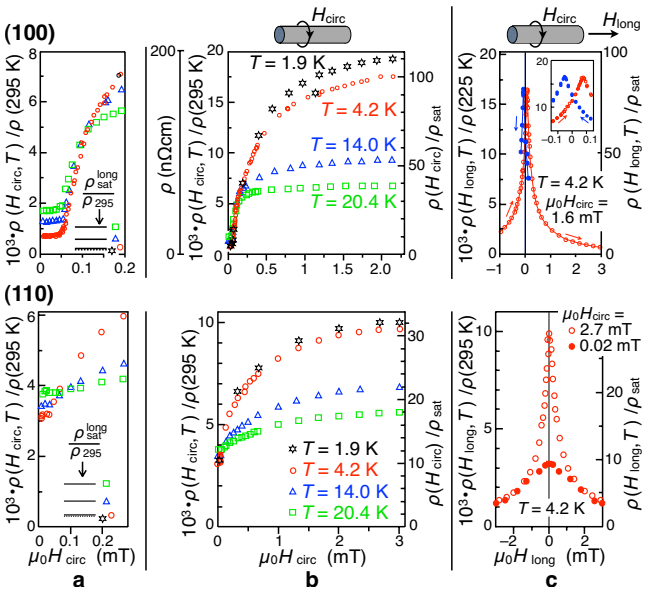

FIG. 3. (Color online) Two similar sets of resistivity curves, measured on the (100) crystal (top, sample 85) and (110) crystal (bottom, sample 87). (a) Resistivity dependence on small circular self-field H_{circ} for different temperatures. (b) Like (a) but for larger circular fields. (c) Resistivity dependence on longitudinal field with circular fields superimposed.

stress-free infinite crystal (which roughly applies to our bulk sample) and at zero field, 1/3 of the volume is occupied by ±90° domains and 2/3 by ±45° and ±135° domains. The occupancy of the two main axes is visible in Fig. 4(b). This relative distribution of the domain phase volumes will also apply to the zero-field state of Fig. 3(a), where the resistance was measured with small currents, i.e., at $H_{\mathrm{circ}} < H_{\mathrm{coercive}}$. The resistivity of this multidomain domain state is by a factor of ten higher than that of the longitudinally saturated state. The reason for this resistivity jump is the creation of a high transverse LMR which is caused by both, the ±90° domains and, to a somewhat lower degree, the ±45° and

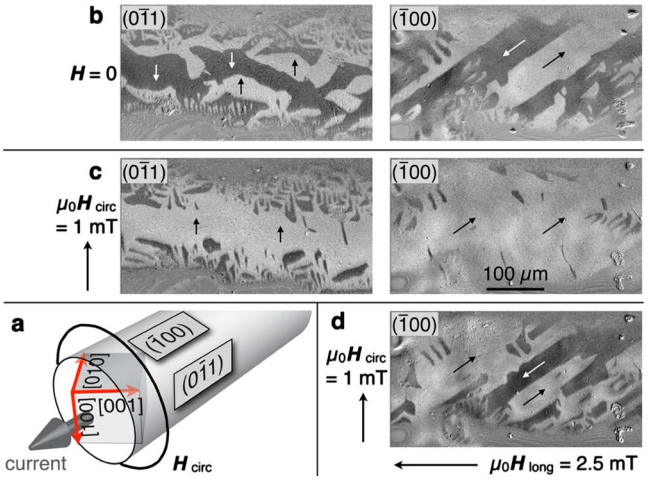

FIG. 4. (Color online) Surface domains of the (110) crystal (sample 87), observed on two surfaces for applied fields as indicated.

$\pm 135°$ domains. The phase volume of the $\pm 45° / \pm 135°$ domains will also contribute a longitudinal LMR, which, however, can only play a minor role for the total resistance of the multidomain state: due to their "short-cutting" effect of the resistivity, the longitudinal LMR of these domain phases should lead to an overall sample resistance that is in the same order of magnitude as that of the longitudinally saturate state. As this is not observed, we can conclude that the *transverse* LMR of the $\pm 45° / \pm 135°$ phase volume will thus dominate the resistance in the zero-field multidomain state.

When a circular field of only 2 mT is applied to this multidomain state, the resistivity strongly rises [Fig. 3(b)], accompanied by a change in the domain structure [Fig. 4(c)]: domains with magnetization components parallel to H_{circ} grow on expense of antiparallel domains. This leads to a reduction in the wall density at a stable transverse MR situation [$B^2_{\mathrm{trans}} = M^2 \sin^2(45°) = M^2 \sin^2(-45°)$, see Eq. (3) below]. The disappearance of domain walls must consequently be responsible for the resistivity rise. A conceivable (though not observed) partial phase transition from $\pm 45°$ to $\pm 90°$ domains, which would also lead to an increasing transverse LMR, can only play a marginal role (this fact is supported by resistivity measurements on a (111)-oriented crystal presented at the end of this section).

If a longitudinal field of just 1 mT is added to the circular field, the 180° walls that separate the $\pm 45°$ or $\pm 135°$ domains reappear again [Fig. 4(d)]. They are formed to create domains with an $\boldsymbol{M}$ component along the field direction to allow some net longitudinal flux. The formation of 180° walls causes a redistribution of the domain phase volumes: the +45° and +135° volume is partly replaced by −45° and −135° volume, whereas the $\pm 90°$ phase volume will stay largely unchanged (we could experimentally prove that the {110} surfaces stay saturated in the superimposed longitudinal field). Again, there is no significant redistribution of the (LMR-relevant) *absolute* $|90°|$ and $|45°|/|135°|$ phase volumes in the superimposed field. The resistivity, however, drops almost down to that of the longitudinally saturated state [compare Figs. 3(b) and 3(c)]. If the redistribution of 90° and $45° / 135°$ phases would be responsible for this drop, the resistance should only decrease by a factor $\ll 2$ [according to Eq. (3) below], but not by (at least) an order of magnitude as measured. Again, it must be the domain walls that are responsible for the effect.

Domain studies on the (100) crystal (Fig. 5) lead to the same conclusion. From the saturated to the zero-field state the resistivity rises [Fig. 3(a)] due to some transversely magnetized volume (see Appendix A). A circular field enforces an ordered structure that consists of ~50-μm-wide slice domains magnetized transverse to the rod axis [Figs. 5(b) and 5(c)]. Due to the transverse LMR, they are responsible for the drastic resistance increase measured in Fig. 3(b). In a superimposed longitudinal field [Fig. 5(d)] the transverse slice state is preserved—the slices are rather tilted and interconnected by further domains. This indicates the formation of obliquely running internal domain walls (see Appendix A), which must be responsible for the drastic resistance decrease in the superimposed longitudinal field [Fig. 3(c)].

For the (110) crystal we have argued that a phase redistribution between $|90°|$ and $|45°|/|135°|$ domain phases in the

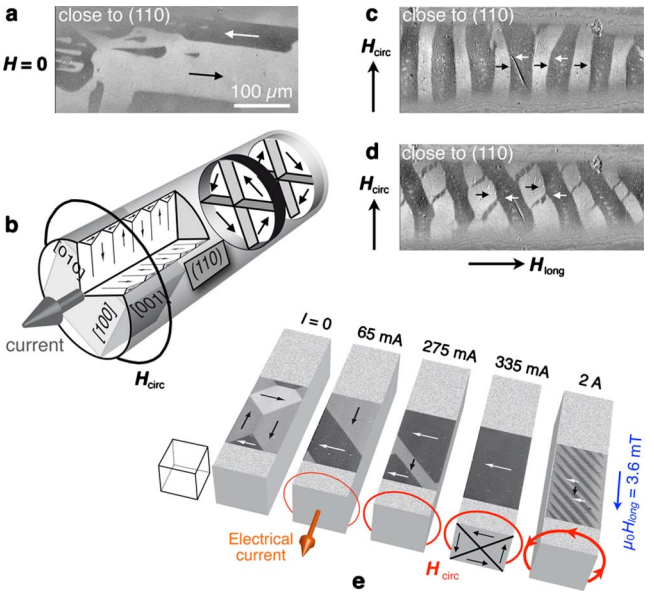

FIG. 5. (Color online) (a) Zero-field domains, observed at a (110) surface of the (100) rod (sample 85, diameter 1 mm). (b) A circular field enforces slice domains with flux-closing surface domains. The segmental cut (left) shows the projection of the magnetization on the cut surfaces (the basic-domain vectors are actually aligned along the [010] axis). Two neighboring basic domains are indicated, drawn apart for clarity. (c) Observation of the closure domains at a (110) surface in accordance with the model in (b). A current of 4 A was applied, creating a transverse circular field $\mu_0 H_{\mathrm{circ}} \approx 1.6$ mT at the rod surface. (d) An additional longitudinal field $\mu_0 H_{\mathrm{long}} \approx 1.1$ mT causes obliquely oriented domain walls. (e) Domain structure of a 220-μm-thick (100)-iron whisker with increasing current (i.e., circular field) and superposition of a longitudinal field (right image).

circular and longitudinal fields would, in principle, result in a change in the LMR, which, however, cannot be significant. For the (100) crystal the situation is different: here any phase reordering between the strictly transverse and strictly longitudinal phases would cause more or less significant LMR effects. The rise of resistivity with increasing circular field [Fig. 3(b)] is to a certain degree in fact caused by such phase transition. The drop of resistivity by a factor of almost 100 in the superimposed longitudinal field [Fig. 3(c)], however, can only be caused by the creation of obliquely running domain walls in an otherwise transversely magnetized volume (Appendix A). There are no indications of a significant growth of longitudinal phase volume on expense of transverse volume, which would, in principle, be possible and LMR relevant for the (100) rod.

So for both crystals our claim is that the huge resistivity changes, occurring in small magnetic fields, are to a large degree due to changes in the domain wall density, whereas phase reordering does not play a significant role. This fact is further and even unambiguously supported by resistivity measurements on a (111)-oriented crystal rod (Fig. 6): for this crystal any kind of domain phase rearrangement (apart from those connected to magnetization rotation) will lead to the same LMR configuration for symmetry reasons, as all easy crystal axes have the same absolute angle relative to the

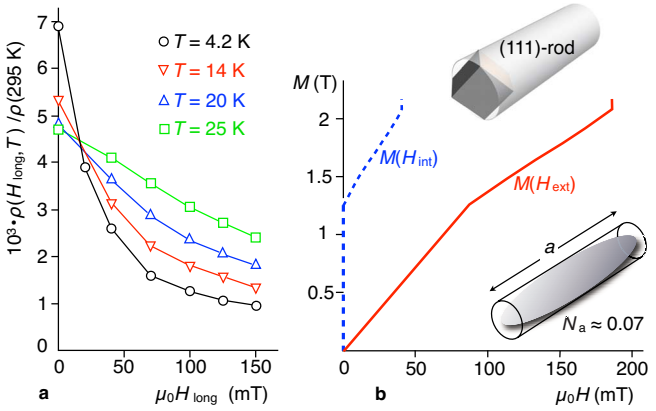

FIG. 6. (Color online) Resistance and magnetization data of a (111)-oriented crystal (RRR=1050). (a) Resistance dependence on externally applied, longitudinal magnetic field for various temperatures. (b) Dashed (blue online): calculated magnetization curve for an infinite iron crystal with field along a (111) axis (after Ref. 17). Full line (red online): sheared magnetization curve, derived from the blue curve by considering a demagnetization factor of 0.07 according to the real crystal dimensions (rod diameter: 4 mm, length: 17 mm). The coercive field, which is around 0.05 mT, was ignored in (b). Note that for the other samples in Fig. 3, which had lengths larger than 3 cm and diameters of 1–1.3 mm, the longitudinal demagnetizing factors are negligibly small so that these samples can be magnetized in very small applied fields.

current direction. Nevertheless, in small magnetic fields similarly drastic resistivity changes are measured as for the other crystals [Fig. 6(a)] and also the temperature dependence of resistivity [Fig. 2(a)] has the same characteristics and order of magnitude. Note that the knee of the magnetization curve in the (111) rod occurs around an external magnetic field of 100 mT [Fig. 6(b)]. Up to this field, phase reordering dominates the magnetization process, and beyond the knee magnetization rotation out of the easy crystal axes does occur. The resistance, however, has already considerably dropped before the knee is reached according to Fig. 6(a). The resistance drop can consequently not be explained by domain phase reordering and rotational processes. Again, there is only the difference in domain wall density left as an interpretation—changes in the longitudinal LMR components can be excluded for (111) crystals. Resistance effects in (111)-oriented iron whiskers,[18] which were found back in the 1970s and which remained unexplained at that time, can be interpreted along the same line.

V. INTERPRETATION AND MODEL

The key to interpret the huge resistivity changes are the *geometrical dimensions* of the Lorentz trajectories of the conduction electrons in real space. They can be derived from fermiology. The conductivity of iron is dominated by the Fermi surface (FS) of the sixth majority-band sheet, shown in Fig. 1(c). The cyclotron orbits at the FS, caused by the Lorentz force, are transferred to helixlike trajectories around the induction B (respectively, magnetization M) in real space with an average diameter d of 5 μm [Fig. 1(b)]. As the mean-free electron path λ in our perfect crystals can be up to 140 μm at low temperature (compared to $\sim$16 nm at room temperature, see Appendix B) a spiral trajectory makes several turns N before scattering. Thus the so-called "high-field limit" $2\pi N = 2\lambda / d_{\max} = \omega_c \tau \gg 1$ is realized (ω_c is the cyclotron frequency and τ the relaxation time). Then for $\Delta\rho_{\text{Lorentz}}$ [Eq. (1)] theory[5–7] yields

$$\Delta\rho_{\text{trans}}(B,T)/\rho(B=0,T) \propto (\omega_c\tau)^2 \propto B^2/\rho(B=0,T)^2, \quad (3)$$

$$\Delta\rho_{\text{long}}(B,T) = c_1\rho(B=0,T). \quad (4)$$

These equations for the transverse and longitudinal LMR hold for compensated metals (i.e., equal numbers of electrons and holes) with closed FS sheets, which both applies to iron. According to Eq. (3), ρ_{trans} unboundedly increases with the number of orbits at the FS, which was indeed measured up to $B=\mu_0(H+M)\cong 20$ T.[19,20] The temperature dependence of the transverse LMR is determined by $\rho(B=0,T)$ in the denominator of Eq. (3) (the numerator stays constant for a stable domain configuration with total or partial transverse M components). Note that in ferromagnetic iron $B=\mu_0 M$ and therefore $\rho(B=0)$ is unknown. In literature, it is usually approximated by $\rho_{\text{long}}(B=\mu_0 M)$, i.e., in our case by the lower set of curves in Fig. 2(a). An estimation of the "true" $\rho(B=0)$, including the saturation factor c_1 in Eq. (4), is presented in Appendix C. In any case, the denominator in Eq. (3) decreases with falling temperature, explaining the negative temperature coefficient (TCR) of the transverse LMR that is measured in Fig. 2(a) (upper set of curves) and in Fig. 3(b).

Such behavior, however, can only occur if the electron helices propagate within sufficiently wide domains, as they are imaged in Figs. 4(c) and 5(c). If a helix interacts with a domain wall, the Lorentz force changes and the spiral trajectory is interrupted. So within an effective width around the wall, given by roughly twice the average helix diameter, full helix turns cannot be formed. Instead, short Lorentz trajectories, wiggling around the wall, will be generated [Fig. 1(d)]. They are equivalent to highly conductive current channels along the wall, which may shortcut the transverse LMR (and to a lower degree also the longitudinal LMR) if the walls have longitudinal orientational components. For our (110) and (100) crystals this scenario is supported by domain observation: the angles between domain magnetization and electrical current direction stay largely constant in the low- and high-resistivity states [i.e., the last term in Eq. (3) remains unchanged], just the number of walls is different (magnetization rotation, which could eventually cause a change in resistance-relevant longitudinal magnetization components, can be excluded or the small applied fields). The huge resistivity changes must consequently be caused by the creation and annihilation of domain walls. Within the channels the negative TCR of Eq. (3) cannot dominate the total resistivity in Eq. (1). The TCR thus changes sign from negative to positive [Fig. 3(a)] when the wall density increases with decreasing circular field.

Encouraged by our discovery, we have revisited the pioneering resistivity studies on Fe whiskers.[18,20,21] Like in Fig. 3(c), a resistivity decrease in a longitudinal field was found. Due to the lack of domain observation, the existence of a

longitudinal core domain in an otherwise transversely magnetized (100) whisker was claimed to cause the drop according to Eq. (4). Our whisker images in Fig. 5(e), however, favor the NDWR channeling as explanation. The NDWR model seems also suitable for differently oriented whiskers [like the (111) whiskers mentioned previously] where the resistance drop could not be explained at all.[18]

VI. SUMMARY AND CONCLUSIONS

To summarize, our resistivity studies (and the related whisker experiments) can only be explained conclusively by assuming that domain walls decrease the LMR, thus causing a NDWR. This "channeling" effect of walls, which is due to a change in the Lorentz trajectories and which is therefore a consequence of fermiology at the end, can drastically exceed any (positive) DWR based on the carrier spin or diamagnetic models.[22–25] It is caused by the electron *charge* and thus independent of spin/wall interactions, being valid for both, electron transmission with spin tracking[26] or reflection with spin conservation.[27] The NDWR is huge at low temperatures, favored by the electronic structure of iron (compensation and closed FS sheets). The measurable features will be weaker, e.g., in Co or Ni and in samples with reduced dimensions (like films) where the surfaces, which act like walls on the Lorentz trajectories,[28] are dominating.[29] Also at higher temperatures the NDWR effect will be reduced and most likely not be strong enough to be isolated from other MR or DWR effects. Nevertheless it is expected that the NDWR plays a role for all domain walls in any kind of magnetic material. Domain walls generally decrease the LMR, and because the LMR is inherent in every ferromagnet with more or less intensity, a *negative domain wall resistance* term exists as a matter of principle and has to be taken into account in any resistivity discussion. This effect was overlooked so far.

ACKNOWLEDGMENTS

Thanks to numerous co-workers in the previous "Institut für Metallphysik und Reinstmetalle" in Dresden, who produced and characterized the excellent iron rods years ago, especially to G. Weise and R. Scharfenberg. The engaged collaboration ofI Kiwitz is gratefully acknowledged. D.E. thanks the head of the Institute for Solid State Physics at IFW Dresden, B. Büchner, for the possibility to finish this work in his institute, and R.S. is grateful to the head of IFW Dresden, L. Schultz, for perpetual support.

APPENDIX A: AUXILIARY DOMAIN OBSERVATIONS ON (110) CRYSTAL

1. Zero-field state: The lancet pattern

On an ideally oriented {110} surface of the (100) rod one would expect domains that are homogeneously magnetized along the surface-parallel easy axis [see Fig. 7(a) for the orientation of the easy axes]. Experimentally observed, however, is the so-called lancet pattern.[17] Examples, imaged on two different {110} surfaces in the zero-field state, are presented in Fig. 7(b). The reason for the lancet formation is a slight misorientation of the [001] axis relative to the rod surface by some degrees. Lancets are shallow surface domains that collect the net magnetic flux, which would otherwise emerge from the surface due to the misorientation. By internal transverse domains the flux is transported to a suitable surface or interface (i.e., a basic domain wall in the interior) of opposite polarity and distributed there again. The sketch in Fig. 7(c) indicates the hidden domains underneath a slightly misoriented {110} surface.

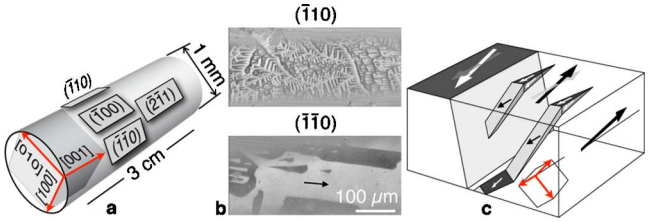

FIG. 7. (Color online) Lancet pattern. (a) Indication of easy crystal axes and selected surfaces on the (100)-oriented iron rod. (b) The lancet domains, imaged on two {110} surfaces, indicate a slight misorientation of the crystal. The density of lancets depends on the degree of the relative misorientation (Ref. 17). (c) The model shows the internal transverse domains that are connected to the surface lancets (after Ref. 17).

The presence of the lancet pattern indicates that in the zero-field (multidomain) state most of the volume of the (100) rod is magnetized longitudinally but that there is also some transversely magnetized volume. The latter is responsible for the moderate resistivity increase measured at zero field compared to the longitudinally saturated state [see Fig. 3(a)].

2. Development of the slice pattern

An electric current J, sent through the (100) rod to measure the resistance, generates a circular magnetic field (Fig. 8) that will favor the transverse easy axes. If the magnetization follows these axes there appears an inherent surface misorientation around the rod, which oscillates between 0° on the {100} surfaces and 45° on the {110} surfaces thus periodically generating magnetic poles [Fig. 8(a)]. To avoid the poles, nature prefers to develop a flux-closed domain pattern, consisting basically of slice domains with alternating clockwise and counterclockwise net magnetization [Fig. 5(b)]. The slices of opposite rotation sense are separated by 180°

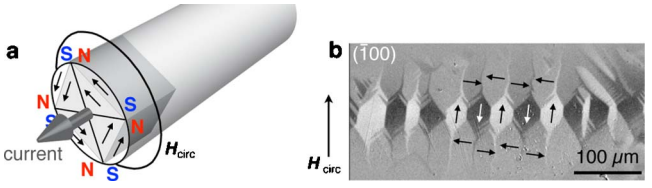

FIG. 8. (Color online) (100) rod in circular field. The magnetic poles in (a) are avoided by slice domains [see Fig. 5(b)] which can be directly seen on the (100) surface (b) See Fig. 5 for more information.

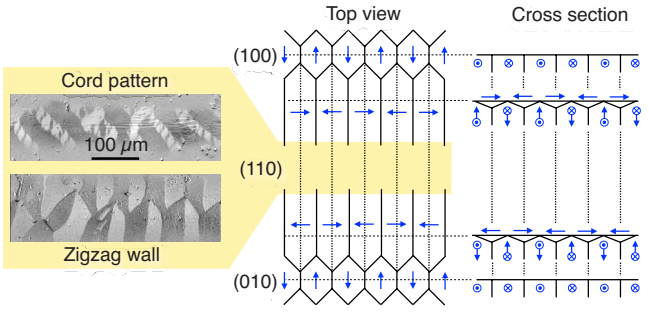

FIG. 9. (Color online) Slice pattern between two {100} surfaces. The top-view sketch indicates the basic domains by dashed walls together with the closure domains. At the (110) surface, topology requires a transition of the closure domains that can be realized by a cord pattern or a zigzag pattern.

domain walls that can be shifted in order to provide flux transport in the direction of the circular field. Each slice domain with a width of about 50 μm is made up of four easy-axis subdomains that are separated by 90° domain walls with a length of roughly 500 μm (the rod radius). These subdomains are the basic domains when a current of some ampere is flowing. On the {100} surfaces the basic domains are directly seen [Fig. 8(b)]. With increasing misorientation they dive below the surface, covered by surface closure domains that are magnetized along the surface-parallel longitudinal easy axis [Fig. 5(c)].

The model of the slice domain pattern, shown in Fig. 5(b), is simplified as it is supposed to emphasize just the transverse magnetization of the basic domains. A more detailed model of the pattern, in a rod segment between two {100} surfaces, is presented in Fig. 9 together with characteristic domain images. At the [001] edge, which is equivalent to a (110) surface [compare Fig. 7(a)], the closure domains have to be shifted in order to adapt to the topology of the basic domains. Two possibilities to realize this shift have been found as shown in Fig. 9: a zigzag wall with a rather abrupt transition and a cord pattern spreading over a certain area around the [001] edge. The cord pattern is explained in the next paragraph.

3. Cord domain pattern

The cord pattern (Fig. 10) is known from (110)-oriented iron or iron-silicon sheets.[17] There it is formed when an in-plane magnetic field is applied not exactly perpendicular to the preferred [001] axis [this is the surface-parallel easy axis that is preferably occupied in a (110)-oriented crystal]. The cord pattern is characterized by tilted surface lines that assume a cordlike appearance [Fig. 10(a)]. If the magnetic field is rotated further away from the transverse direction [Fig. 10(b)], the cords degenerate to oblique lines at the surface. The basic domains of the cord (and line) pattern are magnetized along the two internal easy axes, which are oriented at $\pm 45°$ relative to the crystal surface. As shown in the model of Fig. 10(c), which applies to the line pattern and (in approximation) also to the cord pattern, the basic domains are separated by magnetostrictively compatible (110) walls. In

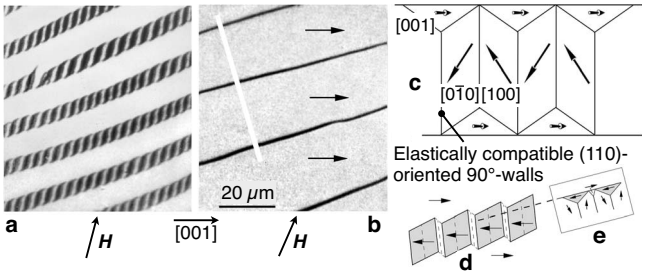

FIG. 10. Fundamentals of the cord pattern. Shown is the observation and interpretation of the cord domain pattern on a (110)-oriented FeSi sheet of 0.3 mm thickness (after Ref. 17). The pattern occurs in an oblique field in which all closure domains are essentially magnetized along the same direction. The two patterns in (a) and (b) can be described by the model in (c), which shows a cross section through the pattern in (b) along the white line. The cord state (a) is schematically explained in (d) and (e). Image (d) shows the top view and (e) the immediate subsurface environment of the cord pattern. For more details see Ref. 17.

this way a high transverse flux is created as required by the strong transverse field component but with little expense of magnetostrictive energy. Most of the closure domains in the cord pattern (and all closure volume in the line pattern), on the other hand, are magnetized along the longitudinal component of the (predominantly transverse) field by following the surface-parallel easy axis. So the cord pattern also allows to transport some longitudinal net flux which is enforced by the misalignment of the transverse field. The overall, oblique orientation of the cord pattern is determined by an equilibrium between wall energy, magnetostrictive interaction energy, and closure energy terms.[17] According to the model in Fig. 10(c), three internal domain walls meet at the surface. The cord pattern is related to a zigzag folding of the internal 90° walls.[17] The zigzag amplitude is enhanced near the surface, thus reducing the volume of the large closure domains. The visible cords represent a secondary closure structure of the enhanced zigzag pattern, as indicated in Figs. 10(d) and 10(e). The essential feature of the cord pattern, which is relevant for the present paper, are the obliquely running 90° domain walls in the volume. They separate the 90° basic domains that are magnetized in transverse direction.

Also in the slice domain state of our (100)-iron rod the cord pattern is observed. As shown in Fig. 9 the cords may help to adapt the displaced closure domains on the {100} surfaces by providing some longitudinal flux. A more pronounced cord pattern develops when in addition to the circular magnetic field (that creates the slice pattern) a longitudinal field is superimposed. Then the cord pattern expands and is also observed in extended neighborhoods around the {100} surfaces [see Fig. 5(d)]. This process is shown in more detail in Fig. 11(a). The cord domains are first formed in the white closure domains, which are magnetized in the direction of the longitudinal field. With increasing longitudinal field, the cords expand on expense of the black closure domains and are finally reduced to oblique lines. In this state, the whole closure volume is magnetized in longitudinal field direction as already indicated in Fig. 10(c). So—enforced by the longitudinal field—the closure domains transport some net flux

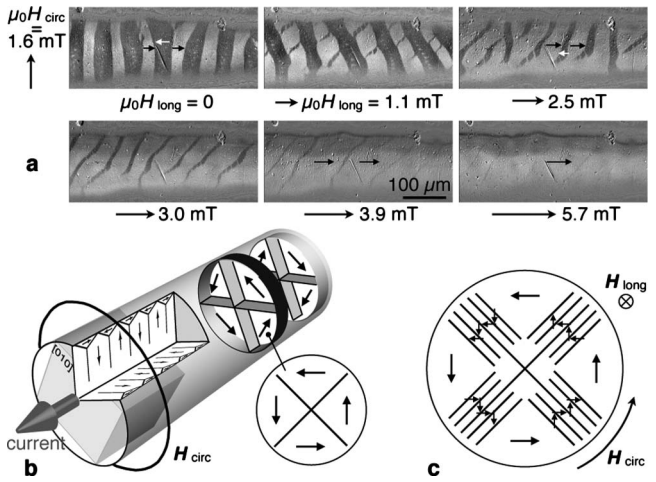

FIG. 11. Development of the cord pattern on (100) rod. (a) Starting from the slice pattern in a circular magnetic field, a cord pattern develops in the white closure domains when a longitudinal field is superimposed. With increasing longitudinal field, the cords transform to oblique line structures. The images were obtained on a surface close to the (110) surface. (b) Model of the slice pattern in a pure circular field (taken from Fig. 5). (c) In a superimposed longitudinal field the number of internal 90° walls increases as can be derived from the formation of the cord pattern.

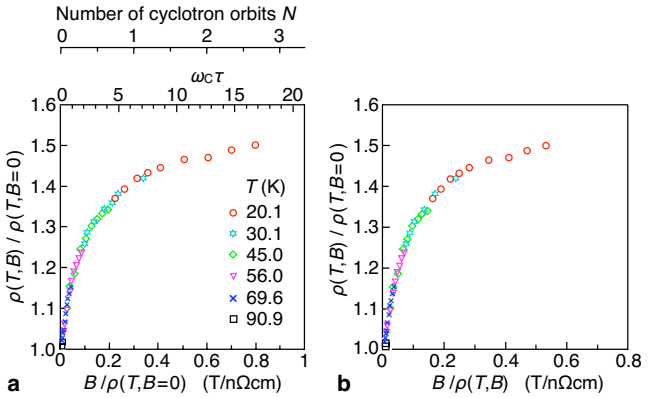

FIG. 12. (Color online) Longitudinal resistance curves for coarse-grained iron polycrystal (RRR=2000). (a) Normalized longitudinal MR versus the reduced field $B/\rho(B=0,T)$, constructed from the $\rho(B,T)$ measurements using Eqs. (C1)–(C3). (b) Normalized longitudinal MR versus $B/\rho(B,T)$, constructed from (a) by dividing the abscissa by the ordinate values. The axes for $\omega_c\tau$ and the number of cyclotron orbits N in (a) are computed by $\omega_c\tau = 2\pi N = \lambda/d$ by using the values in Fig. 1(c) and $\rho\cdot\lambda = 1.62 \times 10^{-11}$ Ω cm^2 (see Appendix B).

in the longitudinal direction, whereas the volume of the (100) rod is still magnetized in transverse direction due to the circular field. As the cord (and line) pattern is inevitably related to the presence of elastically compatible 90°-basic domain walls, our slice model, which applies to the pure circular field and which is shown again in Fig. 11(b), has to be modified in the superimposed longitudinal field as indicated in Fig. 11(c). Around the four 90° walls within each slice, a number of further 90° walls is formed in the volume that run at an oblique angle along the rod axis. At the same time the closure domains are reorganized to create a net longitudinal component. The total closure volume in the cord state is not significantly different to that in the pure slice state.

To summarize Figs. 5(d) and 11: in a superimposed longitudinal field, additional domain walls are created in the rod volume that are oriented at an oblique angle relative to the rod axis. The overall volume of the rod remains transversely magnetized as enforced by the circular field. The additional domain walls are responsible for the drop in resistance, which is evident from Fig. 3(c).

APPENDIX B: ESTIMATION OF MEAN-FREE PATH λ

In Ref. 30 the quantity $\rho\cdot\lambda$, which is for metals determined by the Fermi surface,[31] was estimated for iron by size effect measurements on mainly 1–5-μm-thick iron whiskers to

$$\rho\cdot\lambda = 1.62 \times 10^{-11}\ \Omega\ \mathrm{cm}^2. \tag{B1}$$

In such thin whiskers the inherent magnetoresistance plays a marginal role [compare the magnitude of the orbit diameter in Fig. 1(c)]. Therefore Eq. (B1) should represent the scalar value $\rho\cdot\lambda$ for cubic iron. The advantage of Eq. (B1) is obvious: the knowledge of either term, λ or ρ, for a certain scattering process (or a sum of scattering processes) makes it possible to estimate the respective complement term. So after determining $\rho(B=0,T)$ from Fig. 12 (Appendix C), the mean-free path $\lambda=\rho\cdot\lambda/\rho(B=0)$ can be estimated. For our best crystal no. Fe85 (RRR=5700), for instance, a mean-free path $\lambda\sim 140$ μm at $T=2$ K is obtained from Eqs. (2) and (B1) with $\rho(295\ \mathrm{K}) = 9.71\times10^{-8}$ Ω m, whereas for room temperature we obtain $\lambda \cong 16$ nm.

In principle, not only the mean-free path has to be estimated by $\rho(B=0,T)$, but also the given RRR values in Fig. 2(b), if the RRR is supposed to be a measure for the crystal perfection in comparison with nonferromagnetic elements. For our best crystal no. Fe85, a corrected RRR of about 8500 would even result, as compared to the value of 5700 given in Fig. 2(b).

APPENDIX C: ESTIMATION OF $\rho(B=0)$ FOR IRON

The analysis and quantitative discussion of Eqs. (3) and (4) require the knowledge of $\rho(B=0,T)$. As B is nonzero in iron, this hypothetic value cannot be measured directly. It can, however, be estimated from longitudinal resistivity measurements at different temperatures T and longitudinal B values according to

$$\rho_{\mathrm{long}}(B,T) = \rho(B=0,T) + \Delta\rho_{\mathrm{long}}(B,T). \tag{C1}$$

The procedure is described in Ref. 32 and makes use of Kohlers rule,[31]

$$\Delta\rho(B)/\rho(B=0) = [\rho(B) - \rho(B=0)]/\rho(B=0) = F[B/\rho(B=0)]. \tag{C2}$$

Accordingly, the additive magnetoresistance $\Delta\rho_{\mathrm{long}}(B,T)$ is a function of the "reduced" field $B/\rho(B=0,T)$. On this basis,

$\Delta\rho_{\text{long}}(B,T)$ in Eq. (C1) was estimated for a small range of the reduced field $B/\rho(B=0,T)$ for iron layers.[9] In our work, we have extended the reduced field range by nearly two orders of magnitude to reach the high-field limit, characterized by the saturation constant c_1 in Eq. (4). The resistivity of a coarse-grained polycrystalline iron rod with RRR >2000 was measured in magnetic fields $\mu_0 H$ up to 15 T, and a temperature range from 20 to 90 K was covered. The sample was a perfect cylindrical rod with a diameter of 3.7 mm and a length of 60 mm, which could be mounted exactly parallel to the field in a 16/18 T magnet (by Oxford Instruments©). Five spot-welded current contacts around the circumference at both ends of the rod ensured a constant current density in the cross section of the central part of the sample, where three pairs of voltage contacts around the cylinder were attached. A small measuring current of only 100 mA was injected to prevent sample heating and to ensure a very stable temperature. The induction B within the sample, as the sum of applied field H, magnetization M, and demagnetizing field $N_{\text{dem}} \cdot M$, was computed in the usual way,

$$B = \mu_0(H + M - N_{\text{dem}} \cdot M) \tag{C3}$$

with the demagnetizing factor $N_{\text{dem}} \leq 0.02$ according to Ref. 33. The results are shown in Fig. 12. The B-dependent resistivity branches for the different temperatures were unified to a single curve in Fig. 12(a) using Kohlers rule, Eq. (C2). The use of Eq. (C2) is justified, because scattering is dominated by the temperature, defect scattering plays only a marginal role according to the high RRR. The figure shows that already after one cyclotron orbit the longitudinal magnetoresistance is approximately saturated. A saturation value $c_1 = 0.5$ [see Eq. (4)] can be determined from Fig. 12 for the high-field limit $\omega_c \tau \gg 1$. The curves represent the *orientation-averaged* longitudinal LMR of iron. Nevertheless they should also give a useful approximation to determine the "field-free" resistivity $\rho(B=0)$ for iron single crystals: the knowledge of B according to Eq. (C3) and the measured resistivity $\rho(B,T)$ yields the abscissa in Fig. 12(b) and from the ordinate one obtains $\rho(B=0,T)$.

*r.schaefer@ifw-dresden.de; http://www.ifw-dresden.de

[1] M. N. Baibich, J. M. Broto, A. Fert, F. Nguyen Van Dau, F. Petroff, P. Etienne, G. Creuzet, A. Friederich, and J. Chazelas, Phys. Rev. Lett. **61**, 2472 (1988).

[2] G. Binasch, P. Grünberg, F. Saurenbach, and W. Zinn, Phys. Rev. B **39**, 4828 (1989).

[3] www.physik.tu-dresden.de/~fermisur/

[4] R. McGuire and R. I. Potter, IEEE Trans. Magn. **11**, 1018 (1975).

[5] A. B. Pippard, *Magnetoresistance in Metals*, Cambridge Studies in Low Temperature Physics Vol. 2 (Cambridge University Press, Cambridge, 1989).

[6] I. M. Lifshitz, M. Ia. Azbel, and M. I. Kaganov, Sov. Phys. JETP **4**, 41 (1957).

[7] E. Fawcett, Adv. Phys. **13**, 139 (1964).

[8] J. F. Gregg, W. Allen, K. Ounadjela, M. Viret, M. Hehn, S. M. Thompson, and J. M. D. Coey, Phys. Rev. Lett. **77**, 1580 (1996).

[9] A. D. Kent, J. Yu, U. Rüdiger, and S. S. P. Parkin, J. Phys.: Condens. Matter **13**, R461 (2001).

[10] M. Ziese, Rep. Prog. Phys. **65**, 143 (2002).

[11] C. H. Marrows, Adv. Phys. **54**, 585 (2005).

[12] G. Behr, J. Werner, G. Weise, A. Heinrich, A. Burkov, and C. Gladun, Phys. Status Solidi A **160**, 549 (1997).

[13] G. Weise and G. Owsian, Krist Tech. **11**, 729 (1976).

[14] R. Scharfenberg, Ph.D. thesis, GDR Academy of Sciences, 1975.

[15] The samples date back to one of the predecessor institutes of IFW Dresden, called "Institut für Metallphysik und Reinstmetalle"—Institute for Metal Physics and High-Purity Metals.

[16] *CRC Handbook of Chemistry and Physics*, 89th ed., edited by D. R. Lide (CRC Press Taylor & Francis, Boca Raton, London, New York, 2008).

[17] A. Hubert and R. Schäfer, *Magnetic Domains* (Springer-Verlag, Berlin, New York, 1998).

[18] P. W. Shumate, Jr., R. V. Coleman, and R. C. Fivaz, Phys. Rev. B **1**, 394 (1970).

[19] K. H. Berthel, N. E. Alekseevskij, V. I. Nishankovskij, D. Elefant, and R.-R. Hesske, Proceedings of Colloques Internationaux du CNRS, Paris, 1975, Vol. 242, p. 387.

[20] R. V. Coleman, R. C. Morris, and D. J. Sellmyer, Phys. Rev. B **8**, 317 (1973).

[21] G. R. Taylor, A. Isin, and R. V. Coleman, Phys. Rev. **165**, 621 (1968).

[22] G. G. Cabrera and L. M. Falicov, Phys. Status Solidi B **62**, 217 (1974).

[23] G. G. Cabrera and L. M. Falicov, Phys. Status Solidi B **61**, 539 (1974).

[24] Yu. I. Mankov, Sov. Phys. Solid State **14**, 62 (1972).

[25] Y. V. Zakharov and L. S. Titov, Phys. Solid State **46**, 303 (2004).

[26] L. Berger, J. Appl. Phys. **49**, 2156 (1978).

[27] M. B. Stearns, J. Magn. Magn. Mater. **104-107**, 1745 (1992).

[28] U. Rüdiger, J. Yu, A. D. Kent, and S. S. P. Parkin, Appl. Phys. Lett. **73**, 1298 (1998).

[29] In Ref. 9 a domain wall-induced resistivity decreases in the (1) promille range was reported for iron thin films. This NDWR was explained in terms of a reduced electron surface scattering at the location of domain walls, which interrupt the surface trajectories of the electrons by deflecting them away from the surface. This is an *extrinsic* effect. The NDWR reported in our paper, however, is an *intrinsic* domain wall effect, caused by the change in the electron trajectory within the wall that leads to a (Lorentz) resistivity reduction according to arguments based on fermiology (see Ref. 7). No secondary scattering processes have to be considered for an explanation.

[30] J. Kadlecová, Czech. J. Phys., Sect. B **27**, 1394 (1977).

[31] J. M. Ziman, *Electrons and Phonons* (Clarendon Press, Oxford, 1963).

[32] F. C. Schwerer and J. Silcox, Phys. Rev. Lett. **20**, 101 (1968).

[33] J. A. Osborn, Phys. Rev. **67**, 351 (1945).